Heat transfer enhancement for thermal energy storage using metal foams embedded within phase change materials (PCMs)

C. Y. Zhao*, W. Lu, Y. Tian

School of Engineering, University of Warwick, CV4 7AL, UK

*corresponding author, Email: c.y.zhao@warwick.ac.uk; Tel: +44 (0)2476522339

Abstract

In this paper the experimental investigation on the solid/liquid phase change (melting and solidification) processes have been carried out. Paraffin wax RT58 is used as phase change material (PCM), in which metal foams are embedded to enhance the heat transfer. During the melting process, the test samples are electrically heated on the bottom surface with a constant heat flux. The PCM with metal foams has been heated from the solid state to the pure liquid phase. The temperature differences between the heated wall and PCM have been analysed to examine the effects of heat flux and metal-foam structure (pore size and relative density). Compared to the results of the pure PCM sample, the effect of metal foam on solid/liquid phase change heat transfer is very significant, particularly at the solid zone of PCMs. When the PCM starts melting, the natural convection can improve the heat transfer performance, thereby reducing the temperature difference between the wall and PCM. Even so, the addition of metal-foam can increase the overall heat transfer rate by 3 - 10 times (depending on the metal foam structures and materials) during the melting process (two-phase zone) and the pure liquid zone. The tests for investigating the solidification process under different cooling conditions (e.g. natural convection and forced convection) have been carried out. The results show that the use of metal foams can make the sample solidified much faster than pure PCM samples, evidenced by the solidification time being reduced by more than half. In addition, a two-dimensional numerical analysis has been carried out for heat transfer enhancement in PCMs by using metal foams, and the prediction results agree reasonably well with the experimental data.

Keywords

PCMs; Metal foams; Heat transfer enhancement; Porosity; Pore size; Non-thermal equilibrium; Charging process;

Published in: *Solar Energy* **84**(8), 2010, pp. 1402–1412.

Doi: http://dx.doi.org/10.1016/j.solener.2010.04.022

Cited as: C.Y. Zhao, W. Lu, **Y. Tian**, "Heat Transfer Enhancement for Thermal Energy Storage Using Metal Foams Embedded within Phase Change Materials (PCMs)", *Solar Energy* **84**(8), 2010, pp. 1402–1412.

1. Introduction

Thermal energy storage is of critical importance in many engineering applications. The demand for CO_2 reduction to curb global warming considerably increases the interest in utilizing renewable energy sources, especially solar energy. Due to the discrepancy between solar energy supply and energy demand, a thermal energy storage device has to be used. Thermal energy storage (TES) plays a vital role in solar thermal energy applications in areas such as energy efficient buildings (Tyagi and Buddhi 2007) and solar thermal power plants (Hoshi et al. 2005), and therefore, it has received significant attention. Similar problems arise for waste heat recovery systems where the waste heat availability and utilization periods are different. Thermal energy storage techniques can be classified as sensible heat storage and latent heat storage (Zalba et al. 2003). Latent heat storage is particularly attractive, since it provides a high energy storage density and can store the energy as the latent heat of fusion at a constant temperature (phase change temperature of the corresponding PCM). The various PCMs are generally divided into three main categories from the material composition: organic, inorganic and eutectic compounds, and two groups from their melting temperature: low temperature (< 200 ^{o}C) and high temperature (>200 ^{o}C). The low-temperature PCMs (organic, inorganic or eutectic) are mainly used in waste heat recovery systems and buildings, while high temperature PCMs (inorganic or eutectic) can be used in solar power plants and other high temperature applications. Organic compounds present several advantages at low temperature applications such as non-corrosion, limited supercooling and no phase segregation, therefore, technical grade paraffin, as one of the organic PCMs, has been extensively used as heat storage materials in low temperature applications such as Tyagi and Buddhi (2007) and Zalba et al. (2003).

Phase change materials (PCMs) have been widely used for thermal energy storage systems due to their capability of storing and releasing large amounts of energy with a small PCM volume and a moderate temperature variation (Pasupathy et al. 2000, Mettawee and Assassa 2007, Nayak et al. 2006). However, Most PCMs suffer the common problem of low thermal conductivity, being around 0.2 and 0.5 for paraffin and inorganic salts, respectively, which prolongs the charging and discharging period.

In order to improve the thermal conductivity of phase change materials, extensive investigations have been carried out to improve the thermal response of PCM through

the addition of different high thermal conductivity materials. Mettawee and Assassa (2007) placed aluminium powder in the PCM for a compact PCM solar collector and tested its performance during the processes of charging and discharging. The results showed that significant improvement can be achieved. Some investigators studied the graphite matrix embedded within paraffin, and significant improvement in thermal conductivity was achieved (Mettawee and Assassa 2007, Nayak et al. 2006, Py et al. 2001, Nakaso et al. 2008). One intrinsic problem of a graphite matrix is its anisotropy in that the thermal conductivity depends on the direction. To solve this problem, some metal materials with high thermal conductivities could be used to enhance the heat transfer performance of the PCMs. The effectiveness of metal matrix and finned surface as thermal conductivity enhancers was numerically studied by Nayak et al. (2006). Ellinger and Beckermann (1991) experimentally investigated the heat transfer enhancement in a rectangular domain partially occupied by a porous layer of aluminum beads. They found that the introduction of a porous layer caused the solid/liquid interface to move faster initially during the conduction-dominated regime. However, the overall melting and heat transfer rates were found to be lower with the presence of porous layer due to the low porosity and permeability which severely constrains the mixing heat transfer caused by the convection.

High porosity (usually over 85%) open-celled metallic foams are considered as one type of the most promising materials to enhance the heat transfer due to their high thermal conductivities and high surface area densities. Extensive investigations have been carried out for the heat transfer in metal foams. However almost all the previous investigations worked on the thermal conduction (Calmidi and Mahajan 1999, Boomsma and Poulikakos 2001, Zhao et al. 2004), forced convection (Lee et al. 1993, Calmidi and Mahajan 2000, Kim et al. 2000, Kim et al. 2001, Hwang et al. 2002, Bhattacharya et al. 2002, Zhao et al 2004, Zhao et al 2005, Phanikumar and Mahajan 2002, Zhao et al. 2006, Lu et al. 2006), thermal radiation (Zhao et al. 2004) and flow boiling heat transfer (Zhao et al. 2009). For solid/liquid phase change heat transfer in metal foams, Krishnan et al (2005) numerically investigated the solid/liquid phase change phenomena by using a two-temperature numerical model. So far, to the authors' knowledge, there are few experimental test data published in the open literatures for the latent heat thermal energy storage (Siahpush et al. 2008). In this paper the solid/liquid phase change heat transfer in metal foams is experimentally

investigated, in order to examine the feasibility of using metal foams to enhance the heat transfer capability of phase change materials for use with the low-temperature thermal energy storage systems. In addition, a two dimensional numerical analysis has been carried out, and the prediction results compare with the experimental data.

2. Experimental test apparatus and uncertainty analysis

2.1 Experimental test apparatus

The apparatus used in this study is schematically shown in Figure 1 for charging process (a) and for discharging process (b). A rectangular copper foam (200x120x25 mm in dimension, 10 *ppi* i.e. 10 pores per inch, 95% porosity, with thermal conductivity of copper being 350 *W/m K*, provided by Porvair plc. UK), as shown in Figure 2, was embedded in paraffin wax RT58 (melting temperature 58 ^{o}C, thermal conductivity 0.21 *W/m K*, heat storage capacity 181 kJ/kg measured in temperature range of 48-62^{o}C by the PCM provider *RUBITHERM*). The metal foams were sintered with a copper plate, and an electrical heating film was attached on the bottom surface of the copper plate to provide the continuous uniform heat flux. The input power can be precisely controlled and measured by an electrical power meter (Hameg HM8115-2, accuracy ±0.5%), thus the uniform heat flux can be known based on the plate surface and the input power. Nine thermocouples were placed at different locations inside the PCMs to monitor the transient temperature variation. Three thermocouples were placed on the copper sheet to record the plate temperatures. For data analysis, only the data measured by the four thermocouples (accuracy ±0.1^{o}C) placed in the middle of test sample had been used to exclude the boundary effect. The underneath of the heating surface was insulated with Armflex insulation material and the other surfaces were covered by acrylic sheets which were transparent for observation. The temperatures and the input power would be automatically recorded by a data acquisition system. Thus the heat transfer rate and the thermal storage capacity could be obtained from the analysis of the recorded data. To know the heat transfer enhancement induced by metal foams, the pure paraffin-core (without metal foams) sample was also measured for comparison. The effect of metal-foam structures (cell size and porosity) on solid/liquid heat transfer was also examined. During the discharge process, the bottom surface of the test section had been exposed to three cooling conditions: insulated as in charging process, natural convection and forced convection. As shown in Figure 1(b), the bottom surface (copper plate) of the test section

was put into a wind tunnel and cooled by the forced air convection. In the test the air speed in the wind tunnel maintained at 8 m/s.

2.2 Uncertainty analysis

The uncertainty of the test was also performed in this study by using Eq. (1). The total uncertainty can be attributed to inaccuracies of measurement for input heat flux and temperature, as well as heat loss. With δT_{TC} being ±0.1ºC (±0.43%) for thermocouples, δT_{IMP} being ±0.3ºC (±1.30%) for the temperature measurement tolerance of IMP3595, the uncertainty of power meter being ±0.5%, q_{LOSS} being estimated at 2.5 *W* according to a heat loss coefficient of 3 *W/m K* for natural convection of air, and q_T being 38.4 *W* (1.6 *KW/m*^{2}), the overall uncertainty of the test was estimated at 6.67% by using Eq. (1).

$$U_T = \sqrt{\left(\frac{\delta T_{TC}}{T_{TC}}\right)^2 + \left(\frac{\delta T_{IMP}}{T_{IMP}}\right)^2 + \left(\frac{\delta q_{PM}}{q_{PM}}\right)^2 + \left(\frac{q_{LOSS}}{q_T}\right)^2} \times 100\% \qquad (1)$$

3. Experimental results and discussions

3.1 IR observation

Prior to the detailed measurements using thermocouples, a picture is taken from the uncovered top surface by using an infrared camera (ThermaCAM^{TM}, FLIR A40) as shown in Figure 3. The picture shows the full liquid paraffin state, as the temperature is well above the melting temperature. From the picture, the cellular structure of the metal foam is clearly seen. Figure 3(b) shows the temperature variation along the line drawn in Figure 3(a). Due to the big difference between the paraffin and metal foam solid structures, the temperature exhibits periodic variation over the domain.

3.2 Charging process (melting process)

Figure 4(a) presents the result for a PCM sample with the presence of a piece of metal foam (10 ppi and 95% porosity). It is noted that the wall temperature increases steadily with a similar rate of paraffin during the whole charging process, exhibiting quite different phenomena from the pure PCM sample shown in Figure 4(b). This can be attributed to the high heat conduction through the metal foam solid structures. Even at the solid state for PCM, the heat input at the bottom surface can still be

quickly transferred to the whole domain of PCM through the solid matrix thermal conduction, thereby homogenizing the field temperature profile. In melting process (temperature range of 48-59^{o}C), PCM absorbs a large amount of fusion heat, the temperature still keeps on rising (not a theoretical constant pressure process), but at a much slower pace than that of pure solid or pure liquid state where there is no phase change.

To facilitate the understanding of the heat transfer performance, the transient temperature difference between the heated wall and PCM (paraffin) at different locations (8 mm, 16 mm, 24 mm from the bottom wall surface) is shown in Figure 5 with the variation of time, while the temperature difference variation with the local PCM temperature is presented in Figure 6. Both figures indicate that the transient temperature difference increases in the solid zone, but it drops a few degrees when local paraffin starts melting. After the local PCM completes the transition from the solid to liquid state, the temperature difference lines experience a sharp drop. It can be attributed to the heat transfer enhancement caused by the liquid phase natural convection effect. Also it is noted from Figure 6 that the upper line rises again after the initial drop, whereas the bottom line continuously drops before it is flattened. Since the upper surface exposes to the environment, the rising temperature difference of the top line (24 mm) at the liquid zone is induced by the cooling effect. On the contrary, the decreasing temperature difference of the bottom line (8 mm) is caused by the natural convection enhancement.

Figure 7 shows the effect of heat flux on the temperature difference between the heated wall and the paraffin at the location of 8 mm from the bottom surface. As expected, the temperature difference increases with the heat flux (incoming solar intensity). All four lines for different heat flux exhibit similar behaviours during the charging process.

The effects of metal foam cell size and relative density (1-porosity) are presented in Figure 8. As the metal-foam cell size reduces from 10 PPI (pore number per inch) to 30 PPI for a given relative density 5%, the temperature difference between the heated wall and the paraffin at the location of 8 mm reduces by 50% at the solid zone due to the increase of solid heat transfer area. When the relative density increases from 5%

to 15%, the temperature difference can be further reduced by two third, as the heat transfer is enhanced by twice.

Figure 9 shows the temperature difference variation with time for a pure PCM sample without metal foams. Compared to the result of the metal foam sample shown in Figure 5, the heat transfer trend for charging process is quite different. The temperature difference sharply increases at the initial stage of heating process. This is caused by the low thermal conductivity of pure paraffin wax (0.21 W/m K), so the heat applied to the surface cannot be transferred inside quickly. When the wall temperature rises above the paraffin melting temperature, the solid paraffin near the heated wall starts melting and changes its state to liquid phase. At the liquid phase zone, the natural convection takes place and therefore the heat transfer rate is dramatically increased, thereby continuously reducing the temperature differences until all the paraffin is melted. The effect of natural convection is so significant that the temperature difference at the two different locations is very close. The fluctuation of the temperature difference is caused by the movement of paraffin wax due to the natural convection.

Figure 10 shows the comparison between the pure paraffin sample and two metal-foam samples during charging process. Compared to the results of the pure PCM sample, the effect of metal foam on solid/liquid phase change heat transfer is very significant, particularly at the solid zone of PCMs, as shown in Figure 1. The heat transfer rate can be enhanced by 5-20 times. When the PCM start melting, the natural convection can improve the heat transfer performance, thereby reducing the temperature difference between the wall and PCM. Even so, the addition of metal-foam can increase the overall heat transfer rate 3 - 10 times (depending on the metal foam structures) during the melting process (two-phase zone) and the pure liquid zone.

3.3 Discharging process (solidification process)

During the cooling process, the top and side surfaces of the test sample are covered by the acrylic sheets. The bottom copper sheet is subjected to different cooling conditions, i.e., natural convection (exposed to the environment) and forced convection (put in the wind tunnel). The comparison of temperature difference

between the wall temperature and the PCM temperature at the location of 8 mm from the bottom wall is shown in Figure 11 under the natural and forced convection cooling conditions. The temperature difference under forced convection is much greater than that under natural convections for both the metal-foam sample and the pure PCM sample. It is noted that the lines for the samples with and without metal foams exhibit quite different trend under the forced convection. For the pure PCM sample, the cooling effect is transferred to the inside domain very slowly due to the low thermal conductivity, and this causes the sharp rise of the temperature difference at the initial stage. However for the metal foam sample, the metal foam structure can quickly dissipate the heat from the PCM, thereby leading to the decreasing trend. Similar to the charging process, the temperature difference of the metal foam sample is significantly reduced, implying that the use of metal foams greatly increases the heat transfer performance of the PCM.

4. Theoretical analyses for heat transfer in PCMs

4.1 Problem description

As is shown in Figure 12, PCMs (paraffin wax RT58 is used in this study) are encapsulated in rectangular metal foams. The sample dimensions are L_1 in x-direction and L_2 in y-direction. PCMs that are embedded into metal foams are heated on the bottom side through a constant heat flux q_w provided by an electric heater, and the three other boundaries (left, right and top side) are placed in the atmosphere and incur heat loss into the air, where the heat transfer coefficients are h_1, h_2 and h_3 respectively.

4.2 Governing equations

A two-dimensional heat transfer analysis is carried out for PCMs embedded into metal foams, and the natural convection is not taken into account in this paper. Thus the physical problem can be described by the following equations, and the interested readers can refer to the papers (Tian and Zhao 2009) for the details. Eq. (2) and Eq. (3) show energy equations for metal foams and PCMs respectively.

$$(1-\varepsilon)\frac{\partial T_s(x,y,t)}{\partial t} = \alpha_{se}\left[\frac{\partial^2 T_s(x,y,t)}{\partial x^2}+\frac{\partial^2 T_s(x,y,t)}{\partial y^2}\right]-\frac{k_{int}}{\rho_s C_{ps}}a_{sf}\frac{\bar{T}_s(x,y,t)-T_f(x,y,t)\big]}{d} \quad (2)$$

$$\varepsilon\frac{\partial T_f(x,y,t)}{\partial t} = \alpha_{fe}\left[\frac{\partial^2 T_f(x,y,t)}{\partial x^2}+\frac{\partial^2 T_f(x,y,t)}{\partial y^2}\right]+\frac{k_{int}}{\rho_f C_{pf}}a_{sf}\frac{\bar{T}_s(x,y,t)-T_f(x,y,t)\big]}{d} \quad (3)$$

The terms on the left hand of these two equations above, stand for changing rate of temperature *T* along with time *t*, and they are caused by thermal diffusion (the first terms on the right hand) and interstitial heat transfer (the second terms on the right hand).

The initial temperatures for PCMs and metal foams are both T_0, and they are heated by a uniform heat flux of q_w at the bottom, which are shown by Eq. (4) and Eq. (5) respectively.

$$T_s(x,y,0)=T_f(x,y,0)=T_0 \quad (4)$$

$$k_{se}\frac{\partial T_s(x,0,t)}{\partial y}+k_{fe}\frac{\partial T_f(x,0,t)}{\partial y}=-q_w \quad (5)$$

It is assumed that PCMs have identical temperature with metal foams at the heating boundary (Zhao et al. 2004), which is shown in Eq. (6).

$$T_f(x,0,t)=T_s(x,0,t) \quad (6)$$

The temperatures of PCMs at melting front are T_m (melting temperature of RT58) all the time.

$$T_f\left[S_x(y,t),S_y(x,t),t\right]=T_m \quad (7)$$

Eq. (8) and Eq. (9) show energy balance for PCMs and metal foams on the left boundary.

$$k_{se}\frac{\partial T_s(0,y,t)}{\partial x}+h_1(1-\varepsilon)\left[T_\infty-T_s(0,y,t)\right]=0 \quad (8)$$

$$k_{fe}\frac{\partial T_f(0,y,t)}{\partial x}+h_1\varepsilon\left[T_\infty-T_f(0,y,t)\right]=0 \quad (9)$$

Eq. (10) and Eq. (11) show energy balance for PCMs and metal foams on the right boundary.

$$-k_{se}\frac{\partial T_s(L_1,y,t)}{\partial x}+h_2(1-\varepsilon)\left[T_\infty-T_s(L_1,y,t)\right]=0 \tag{10}$$

$$-k_{fe}\frac{\partial T_f(L_1,y,t)}{\partial x}+h_2\varepsilon\left[T_\infty-T_f(L_1,y,t)\right]=0 \tag{11}$$

Eq. (12) and Eq. (13) show energy balance for PCMs and metal foams on the top boundary.

$$-k_{se}\frac{\partial T_s(x,L_2,t)}{\partial y}+h_3(1-\varepsilon)\left[T_\infty-T_s(x,L_2,t)\right]=0 \tag{12}$$

$$-k_{fe}\frac{\partial T_f(x,L_2,t)}{\partial y}+h_3\varepsilon\left[T_\infty-T_f(x,L_2,t)\right]=0 \tag{13}$$

The above equations can be solved only if *S(x, y, t)* has been given, unfortunately it is unlikely for us to obtain *S(x, y, t)* beforehand. The function, *S(x, y, t)*, which stands for moving melting boundary, is being coupled with *T(x, y, t)*. The correlation between *S(x, y, t)* and *T(x, y, t)* is given by Eq. (14) and Eq. (15), which can be obtained by the Energy Conservation Law.

$$\rho H_L\varepsilon\frac{d\left(S_x(y,t)\right)}{dt}=k_{fe}\frac{\partial T_f(S_x(y,t)^+,y,t)}{\partial x}-k_{fe}\frac{\partial T_f(S_x(y,t)^-,y,t)}{\partial x}+k_{int}a_{sf}\frac{d\left(S_x(y,t)\right)}{dt}\frac{\bar{T}_s\left[S_x(y,t),y,t\right]-T_f\left[S_x(y,t),y,t\right]}{d} \tag{14}$$

$$\rho H_L\varepsilon\frac{d\left(S_y(x,t)\right)}{dt}=k_{fe}\frac{\partial T_f(x,S_y(x,t)^+,t)}{\partial y}-k_{fe}\frac{\partial T_f(x,S_y(x,t)^-,t)}{\partial y}+k_{int}a_{sf}\frac{d\left(S_y(x,t)\right)}{dt}\frac{\left[\bar{T}_s\left[x,S_y(x,t),t\right]-T_f\left[x,S_y(x,t),t\right]\right]}{d} \tag{15}$$

In Eq. (14) and Eq. (15), the terms on the left hand mean marching speed of melting front; The first terms on the right hand denote the heat given by solid zone of PCMs, while the second terms on the right hand denote the heat given by fluid zone of PCMs; The third terms on the right hand mean the heat from metal foams to PCMs. The superscript "+" means the Right Limit in Mathematics, representing solid zone of PCMs, while the superscript "-" means the Left Limit in Mathematics, representing

fluid zone of PCMs. Here Eq. (14) and Eq. (15) denote *x*-component and *y*-component of melting front function respectively.

4.3 Effective thermal conductivity of metal foams

Metal foams have so complicated interior microstructures that it is hard for us to accurately capture the heat transfer phenomena within the foam structures. In this study a three-dimensionally structured model (tetrakaidecahedron) presented by Boomsma and Poulikakos (2001) has been used to deal with the effective thermal conductivity of metal foams, as shown in Eq. (16). The involved details are left out in this paper for brevity, and interested readers could refer to the paper of them (listed in References) for further details.

$$
\begin{aligned}
k_e &= \frac{\sqrt{2}}{2\left(R_A + R_B + R_C + R_D\right)} \\
R_A &= \frac{4\lambda}{\left(2e^2 + \pi\lambda(1-e)\right)k_s + \left(4 - 2e^2 - \pi\lambda(1-e)\right)k_f} \\
R_B &= \frac{\left(e-2\lambda\right)^2}{(e-2\lambda)e^2 k_s + \left(2e - 4\lambda - (e-2\lambda)e^2\right)k_f} \\
R_C &= \frac{\left(\sqrt{2}-2e\right)^2}{2\pi\lambda^2\left(1-2e\sqrt{2}\right)k_s + 2\left(\sqrt{2}-2e-\pi\lambda^2\left(1-2e\sqrt{2}\right)\right)k_f} \\
R_D &= \frac{2e}{e^2 k_s + \left(4-e^2\right)k_f} \qquad \lambda = \sqrt{\frac{\sqrt{2}\left(2-(5/8)e^3\sqrt{2}-2\varepsilon\right)}{\pi\left(3-4e\sqrt{2}-e\right)}} \qquad e = 0.339
\end{aligned}
\tag{16}
$$

4.4 Numerical procedure

A FDM-based (Finite Difference Method) programme has been developed for dealing with the phase change heat transfer problem in PCMs embedded into metal foams aforementioned. The uniform mesh grids are employed, which are 14×112, i.e. 14 for spatial grids of *y*-direction (0.025 *m*) and 112 for spatial grids of *x*-direction (0.2 *m*). Iterations are aborted when the maximum difference between two successive iterations is smaller than 10^{-6}.

4.5 Numerical results and discussions

The numerical results have been compared with the corresponding experimental data, where a piece of rectangular metal foam (200x120x25 mm in dimension, copper foam

of 10 *ppi* and 95% porosity) was embedded in RT58 (melting temperature: 48-62℃, latent heat of fusion: 181 *kJ/kg*, according to the PCMs provider RUBITHERM®).

Figure 13 shows a comparison between numerical results and experimental data. The symbol "*y*" denotes the vertical coordinate of the computational domain, meaning the distance of local positions away from heating wall. Both numerical results and experimental data show that PCMs begin to melt around t = 1200 *s* and finish phase change around t = 4000 *s*, and a good agreement between them has been achieved. It needs to be noticed that the PCMs we used in this experiment are not a sort of proper crystal material with invariable melting point, this RT58 melts in a temperature range of 48-62℃ according to the PCMs provider RUBITHERM®. However in our numerical investigations, PCMs are regarded as a sort of phase change materials with constant melting point so that a relatively flat melting curve is obtained in numerical results. Variable melting point of RT58 makes it impossible to achieve a perfect agreement between numerical results and experimental data, unless the PCMs with fixed melting point are used. As is shown in Figure 13, the temperatures of RT58 increase more slowly than before, this is because the heat provided is mainly used for phase change not for sensible heat increasing. After RT58 has fully become liquid state when temperatures are higher than 62℃, its temperatures begin to increase faster again, this is because the heat provided is not used for overcoming latent heat of fusion any more, and only for sensible heat increasing of PCMs.

5. Conclusions

In this paper the heat transfer enhancement is experimentally investigated by embedding metal foams in the paraffin (RT-58). Compared to the results of the pure PCMs sample, the effect of metal foam on solid/liquid phase change heat transfer is very significant, particularly at the solid zone of PCMs, and the heat transfer rate can be enhanced by 5-20 times. When the PCMs start melting, the natural convection can improve the heat transfer performance, thereby reducing the temperature difference between the wall and PCM. Even so, the addition of metal-foam can increase the overall heat transfer rate by 3-10 times (smaller porosity and pore density results in better heat transfer performance, depending on the metal foam parameters) during the melting process (two-phase zone) and the pure liquid zone. The tests for investigating

the solidification process under different cooling conditions (e.g. natural convection and forced convection) were carried out. Similar to the charging process, the temperature difference of the metal foam sample is significantly reduced, implying that the use of metal foams greatly increases the heat transfer performance of the PCM. In addition, a two dimensional numerical analysis has been carried out for heat transfer enhancement in PCMs by using metal foams, and the prediction results agree reasonably well with the experimental data.

Acknowledgements

This work is supported by the UK Engineering and Physical Science Research Council (EPSRC grant number: EP/F061439/1) and Warwick Research Development Fund (RDF) Strategic Award (RD07110). The authors also wish to thank the assistance of Mr. Ian Stirling, Porvair Plc., for providing test samples.

References

Bhattacharya, A., Calmidi, V. V., Mahajan, R. L., 2002. Thermophysical properties of high porosity metal foams. International of Journal of Heat Mass Transfer 45, 1017 – 1031.

Boomsma, K., Poulikakos, D., 2001. On the effective thermal conductivity of a three-dimensionally structured fluid-saturated metal foam. International of Journal of Heat Mass Transfer 44, 827 – 836.

Boomsma, K., Poulikakos, D., 2001. The effects of compression and pore size variations on the liquid flow characteristics in metal foams. ASME Journal of Fluids Engineering 124, 263-272.

Calmidi, V. V., Mahajan, R. L., 1999. The effective thermal conductivity of high porosity fibrous metal foams. ASME Journal of Heat Transfer 121, 466 – 471.

Calmidi, V. V., Mahajan, R. L., 2000. Forced convection in high porosity metal foams. ASME Journal of Heat Transfer 122, 557 – 565.

Ellinger, E. A., Beckermann, C., 1991. On the Effect of Porous Layers on Melting Heat Transfer in an Enclosure. Experimental Thermal and Fluid Science 4, 619–629.

Hoshi, A., Mills, D.R., Bittar A., Saitoh, T.S., 2005. Screening of high melting point phase change materials (PCM) in solar concentrating technology based on CLFR. Solar Energy 79, 332–339.

Hwang, J. J., Hwang, G. J., Yeh, R. H., Chao, C. H., 2002. Measurement of interstitial convective heat transfer and frictional drag for flow across metal foams. Journal of Heat Transfer 124, 120 – 129.

Kim, S. Y., Kang, B. H., Kim, J. H., 2001. Forced convection from aluminium foam materials in an asymmetrically heated channel. International of Journal of Heat Mass Transfer 44, 1451 – 1454.

Kim, S. Y., Paek, J. W., Kang, B. H., 2000. Flow and heat transfer correlations for porous fin in a plate-fin heat exchanger. Journal of Heat Transfer 122, 572 –578.

Krishnan, S., Murthy, J. Y., Garimella, S.V., 2005. A Two-temperature Model for Solid-liquid Phase Change in Metal Foams. ASME Journal of Heat Transfer 127, 997-1004.

Lee, Y. C., Zhang, W., Xie, H., Mahajan, R. L., 1993. Cooling of a FCHIP package with 100 watt, 1 cm^2 chip. Proceedings of the 1993 ASME International. Electronics Packaging Conference 1, ASME, New York, 419-423.

Lu, W., Zhao, C. Y., Tassou, S. A., 2006. Thermal Analysis on Metal-Foam Filled Heat Exchangers, I. Metal-Foam Filled Pipes. International of Journal of Heat and Mass Transfer 49, 2751-2761.

Marin, J.M., Zalba, B., Cabeza, L. F., Mehling, H., 2005. Improvement of a thermal energy storage using plates with paraffin-graphite composite 48, 2561-2570.

Mettawee, E.S., Assassa, G.M.R., 2007. Thermal Conductivity enhancement in a Latent Heat Storage System. Solar Energy 81, 839-845.

Mills, A., Farid, M., Selman, J. R., Al-Hallaj, S., 2006. Thermal conductivity enhancement of phase change materials using a graphite matrix. Applied Thermal Engineering 26, 1652-1661.

Nakaso, K., Teshima, H., Yoshimura, A., Nogami, S., Hamada, Y., Fukai, J., 2008. Extensin of Heat Transfer Area Using Carbon Fiber Cloths in Latent Heat Thermal Energy Storage Tanks. Chemical Engineering and Processing 47, 879-885.

Nayak, K.C., Saha, S.K., Srinivasan, K., Dutta, P., 2006. A Numerical Model for Heat Sinks with Phase Change Marterials and Thermal Conductivity Enhancers. International of Journal of Heat and Mass Transfer 49, 1833-1844.

Pasupathy, A., R. Velraj, Seeniraj, R. V., 2000. Phase Change Material-based Building Architecture for Thermal Management in Residential and Connercial Establishments. Renewable and Sustainable Energy Reviews 12, 39-64.

Phanikumar, M. S., Mahajan, R. L., 2002. Non-Darcy natural convection in high porosity metal foams. International of Journal of Heat and Mass Transfer 45, 3781-3793.

Py, X., Olives, R., Mauran, S., 2001. Paraffin/porous-graphite-matrix composite as a high and constant power thermal storage material. International Journal of Heat and Mass Transfer 44, 2727-2737.

Siahpush, A., O'Brien, J., Crepeau, J., 2008. Phase Change Heat Transfer Enhancement Using Copper Porous Foam. ASME Journal of Heat Transfer 130, 082301-1-11.

Tian, Y, Zhao, C. Y., 2009. Heat Transfer Analysis for Phase Change Materials (PCMs). The 11th International Conference on Energy Storage (Effstock 2009), June, Stockholm, Sweden.

Tian, Y, Zhao, C. Y., 2009. Numerical investigations of heat transfer in phase change materials (PCMs) using non-thermal equilibrium model. The 11th UK National Heat Transfer Conference (UKHTC 2009), Queen Mary, London, UK.

Tyagi, V. V., Buddhi, D., 2007. PCM thermal storage in buildings: a state of art. Renewable and Sustainable Energy Reviews 11, 1146-1166.

Zalba, B., Martin, J. M., Cabeza, L. F., Mehling, H., 2003. Review on thermal energy storage with phase change: materials, heat transfer analysis and applications. Applied Thermal Engineering 23, 251-283.

Zhao, C. Y., Kim, T., Lu, T. J., Hodson, H. P., 2004. Thermal transport in high porosity cellular metal foams. Journal of Thermophysics and Heat Transfer 18, 309-317.

Zhao, C. Y., Lu, T. J., Hodson, H. P., Jackson, J. D., 2004. The Temperature Dependence of Effective Thermal Conductivity of Open-Celled Steel Alloy Foams. Materials Science and Engineering: A 367, 123-131.

Zhao, C. Y., Lu, T. J., Hodson, H. P., 2004. Thermal Radiation in Metal Foams with Open Cells. International of Journal of Heat and Mass Transfer 47, 2927 – 2939.

Zhao, C. Y., Lu, T. J., Hodson, H. P., 2005. Natural convection in metal foams with open cells. International of Journal of Heat and Mass Transfer 48, 2452-2463.

Zhao, C. Y., Lu, W., Tassou, S. A., 2006. Thermal Analysis on Metal-Foam Filled Heat Exchangers, II. Tube Heat Exchangers. International of Journal of Heat and Mass Transfer 49, 2762-2770.

Zhao, C. Y., Lu, W., Tassou, S. A., 2009. Flow boiling heat transfer in horizontal metal foam tubes. ASME Journal of Heat Transfer 131, 121002-1-8.

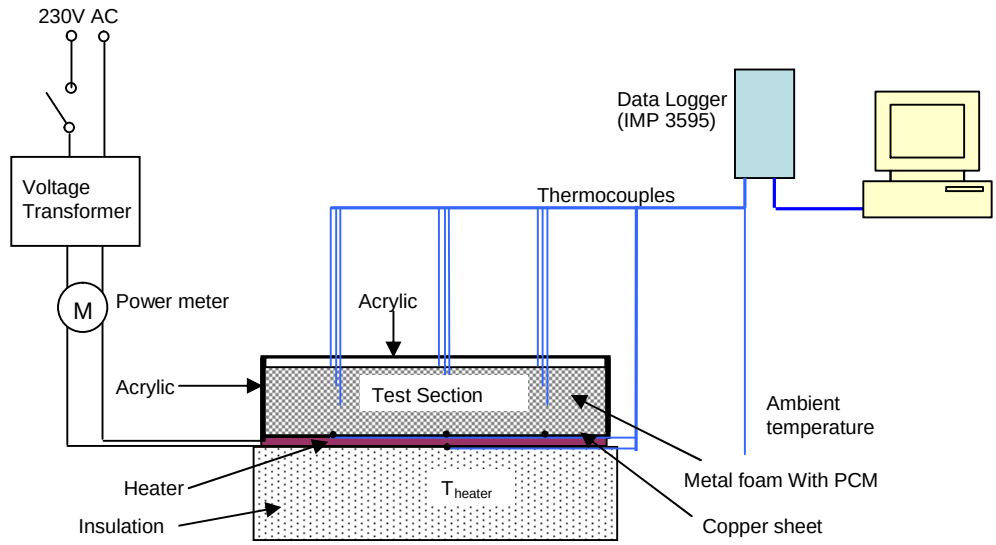

(a) Charging process

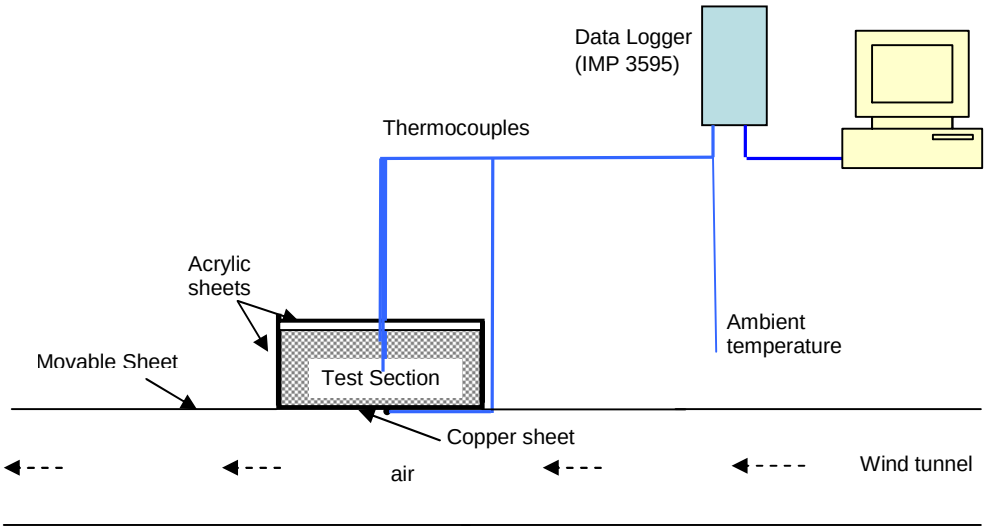

(b) Discharging process

Figure 1 Schematic diagram of the experimental apparatus

Figure 2 A piece of paraffin sample with copper foam embedded

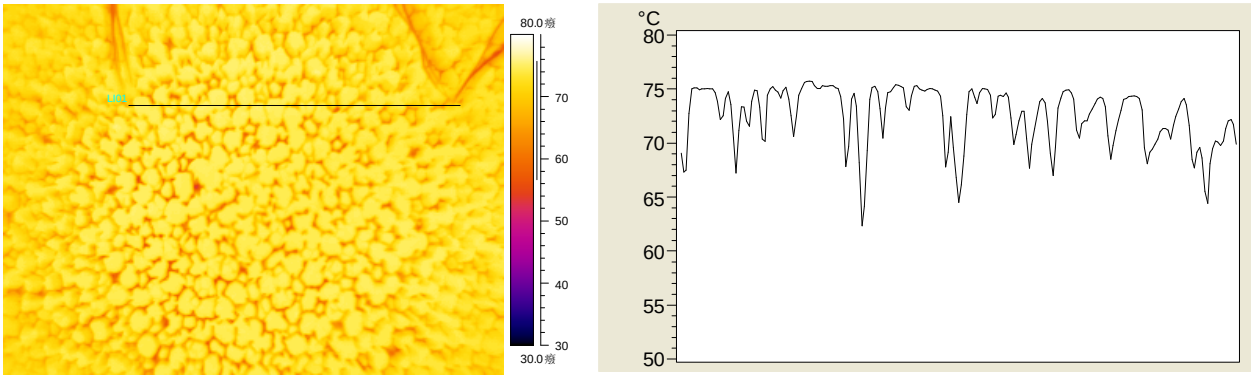

(a) (b)

Figure 3 A picture taken by an IR camera

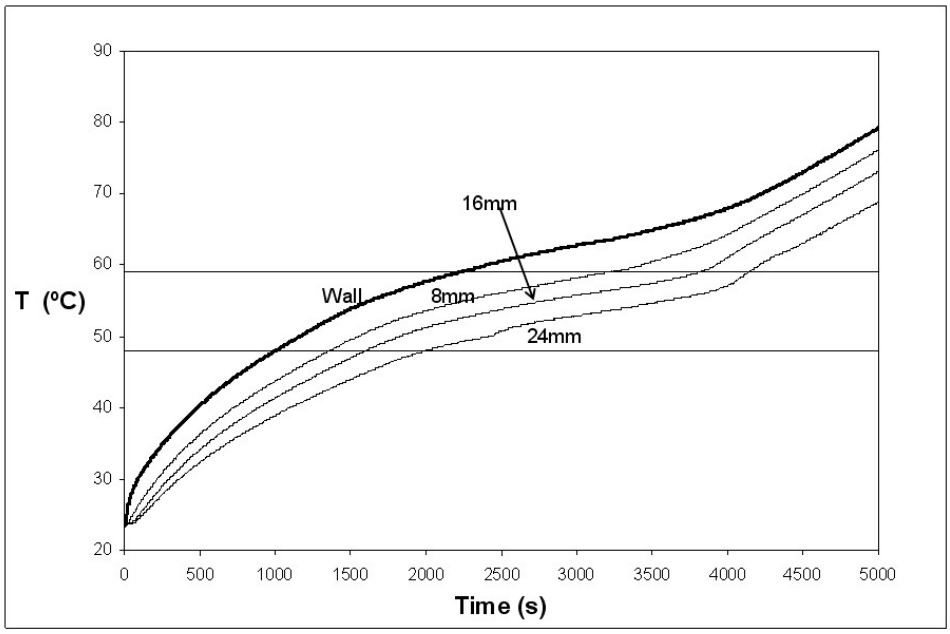

(a) for a metal-foam embedded PCM sample

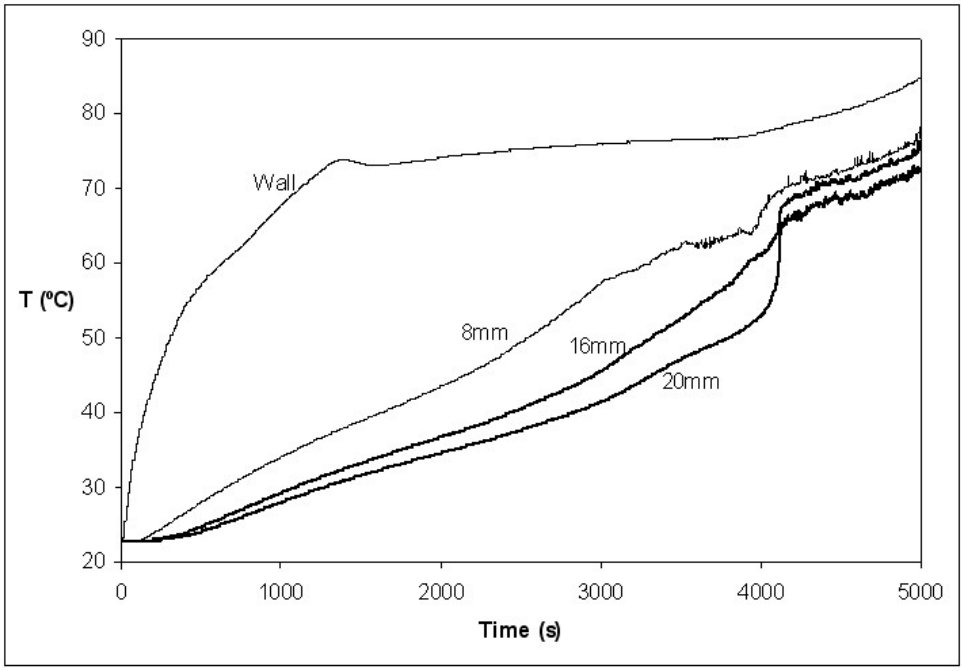

(b) for a pure PCM sample

Figure 4 Temperature variations of the bottom wall and the PCM at different locations during the melting process.

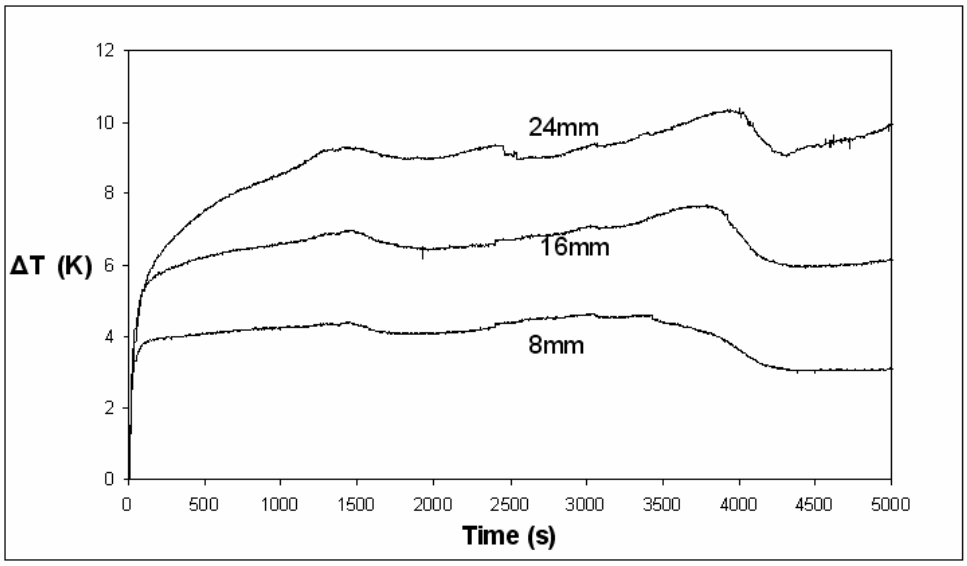

Figure 5 Temperature difference between the heated wall and the PCM at different locations during the melting process (1.6KW/m^2).

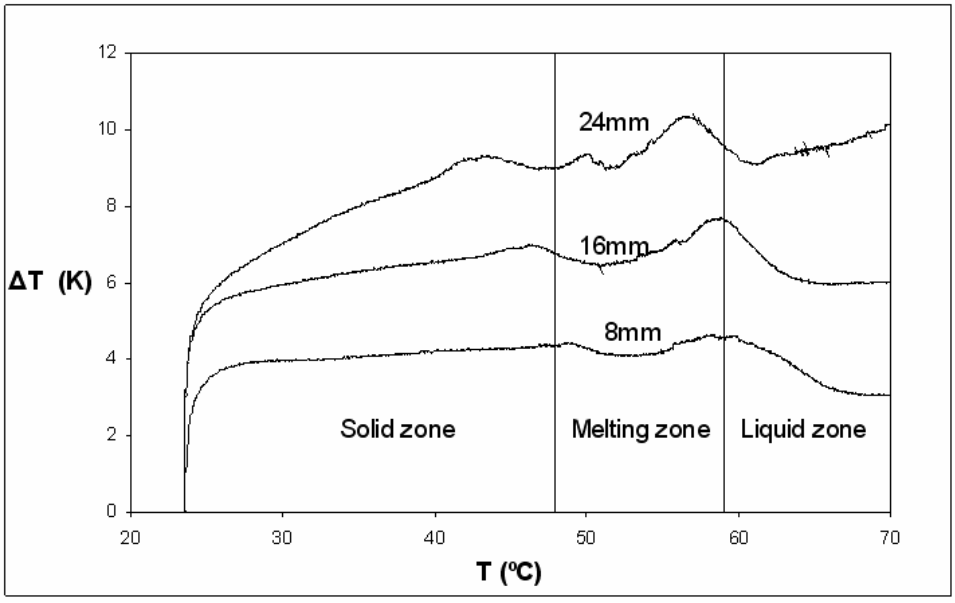

Figure 6 Variation of temperature difference with the local PCM temperature during the melting process (1.6KW/m^2).

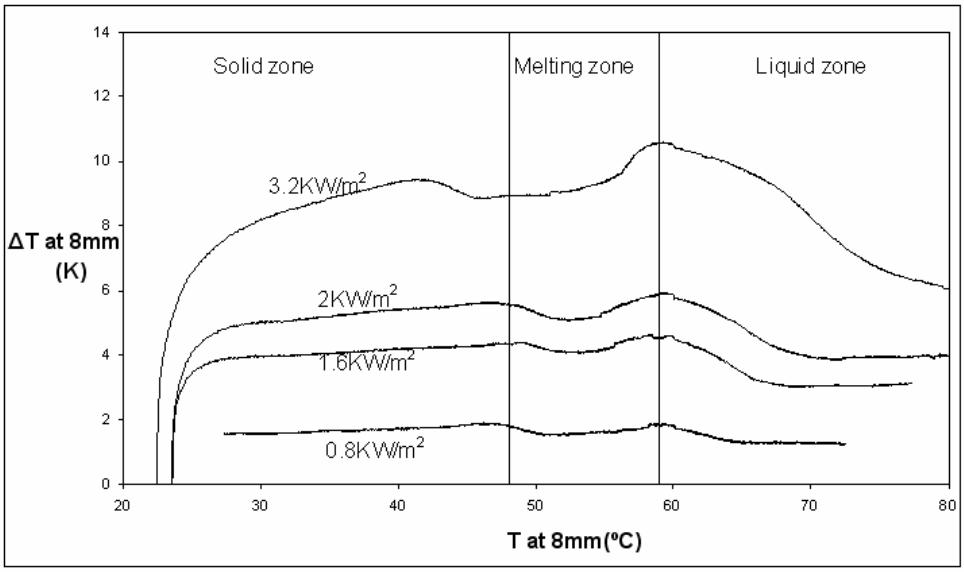

Figure 7 Effect of heat flux on the temperature difference between the heated wall temperature and the PCM temperature at 8mm during the melting process.

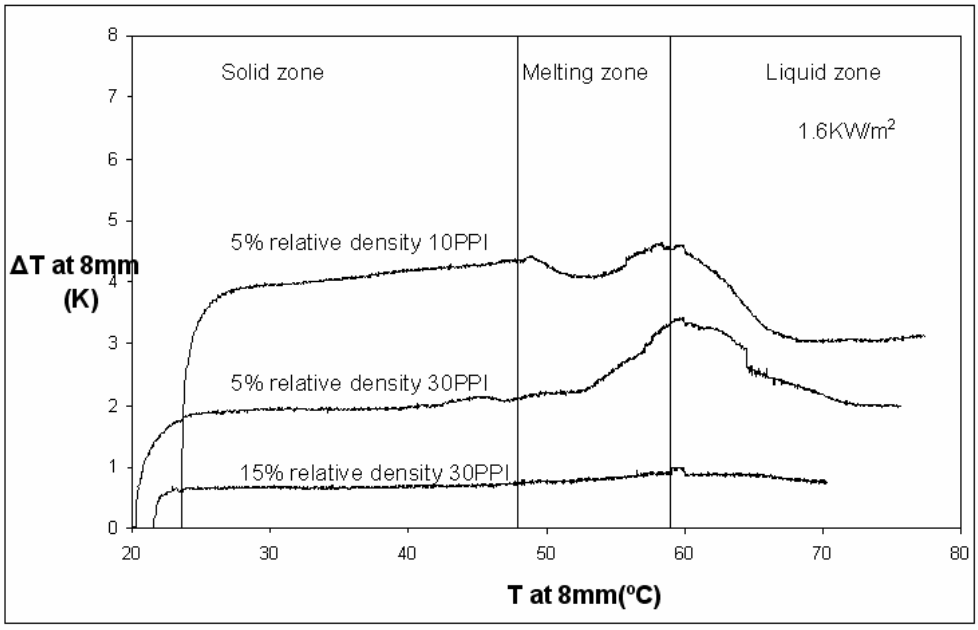

Figure 8 Effect of metal foam structures.

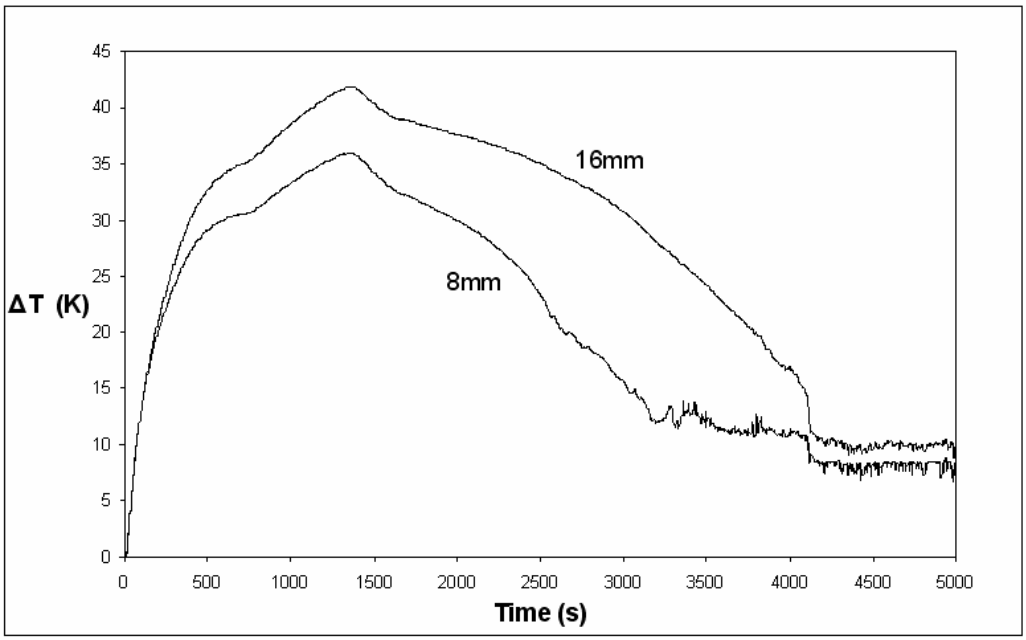

Figure 9 Variation of temperature difference for a pure PCM sample.

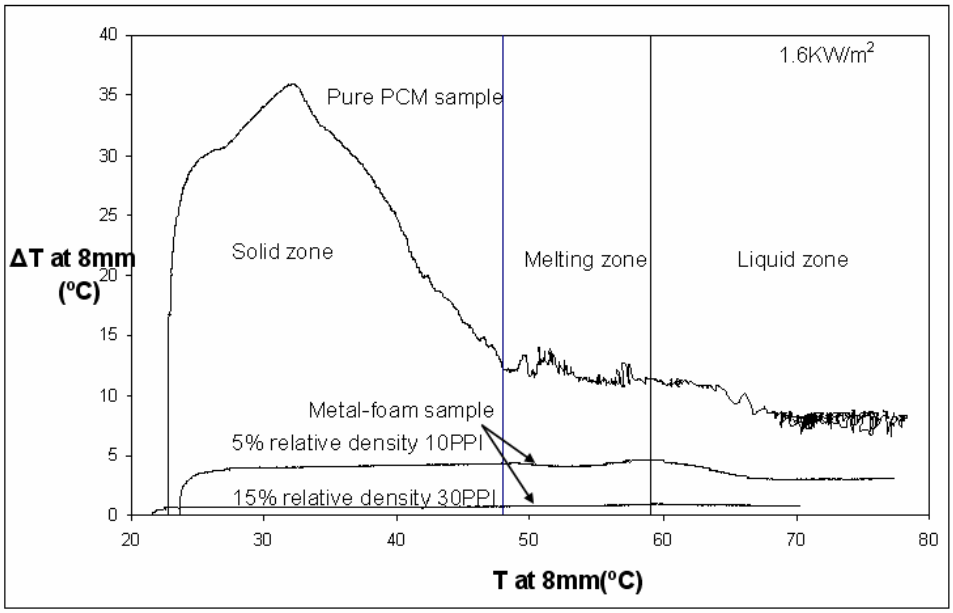

Figure 10 Comparison between the pure PCM sample and metal-foam samples during the charging (melting) process.

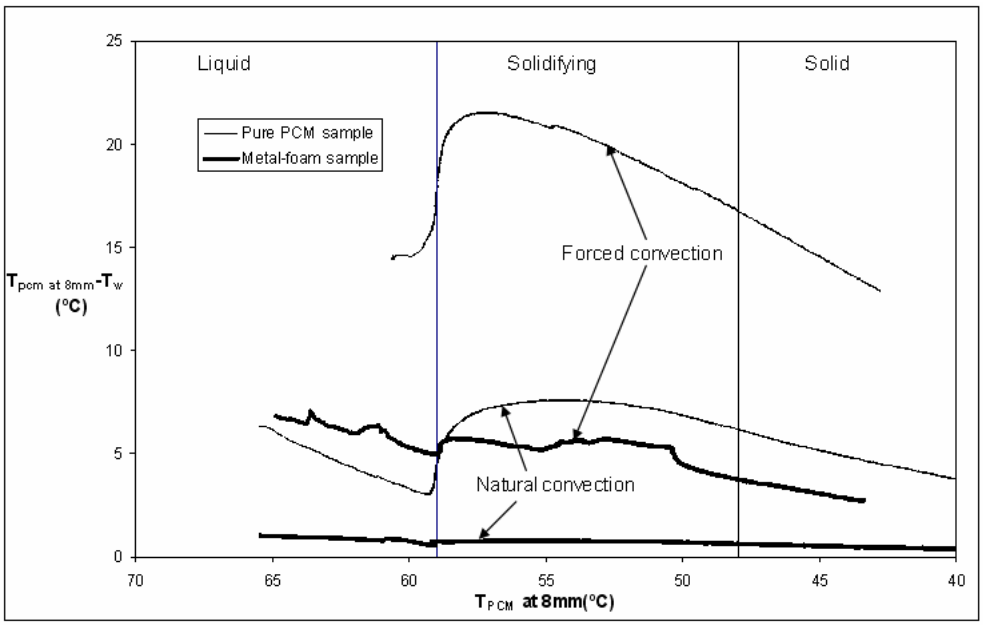

Figure 11 Comparison between the pure PCM sample and metal-foam samples during the discharging (solidification) process.

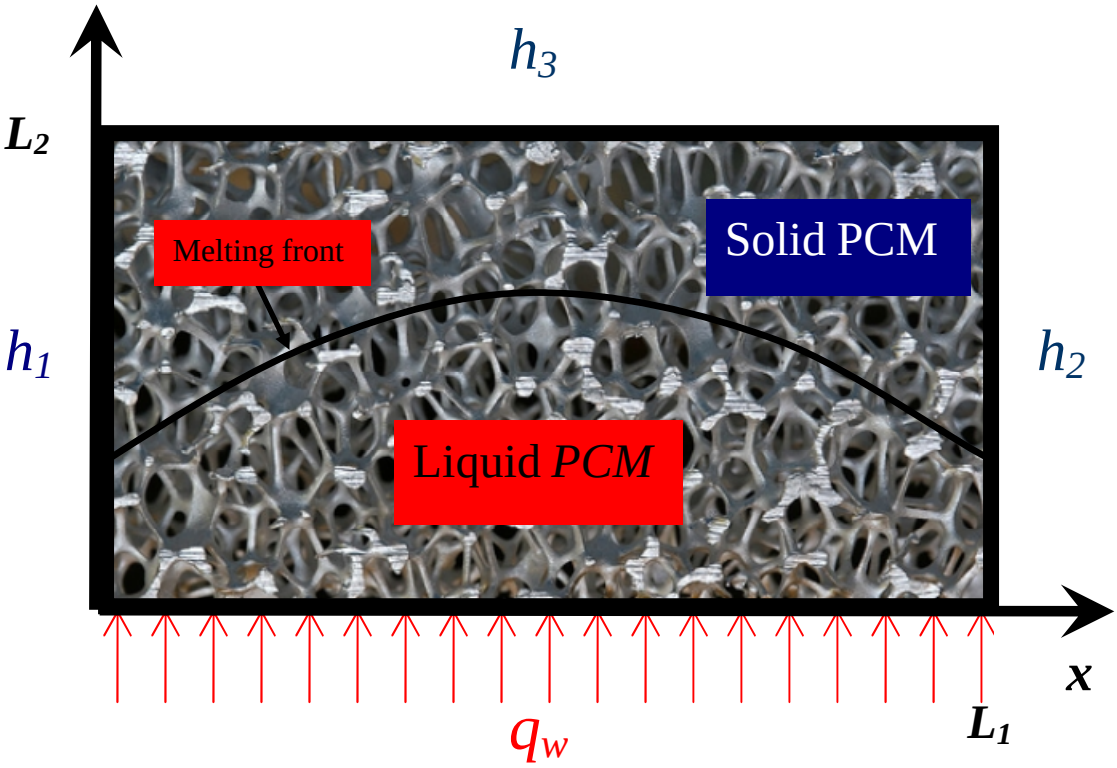

Figure 12 PCMs embedded into metal foams.

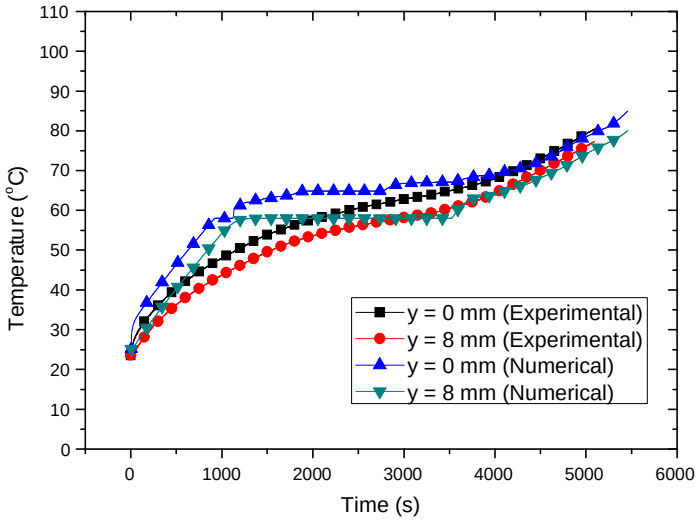

Figure 13 Results of two-equation model compared with experimental data.